

Kent Academic Repository

Full text document (pdf)

Citation for published version

Groucutt, Huw S. and Grun, Rainer and Zalmout, Iyad S. A. and Drake, Nick A. and Armitage, Simon J. and Candy, Ian and Clark-Wilson, Richard and Louys, Julien and Breeze, Paul S. and Duval, Mathieu and Buck, Laura T. and Kivell, Tracy L. and Pomeroy, Emma and Stephens, Nicholas B and Stock, Jay T and Stewart, Matthew and Price, Gilbert J and Kinsley, Leslie and

DOI

<https://doi.org/10.1038/s41559-018-0518-2>

Link to record in KAR

<http://kar.kent.ac.uk/66671/>

Document Version

Author's Accepted Manuscript

Copyright & reuse

Content in the Kent Academic Repository is made available for research purposes. Unless otherwise stated all content is protected by copyright and in the absence of an open licence (eg Creative Commons), permissions for further reuse of content should be sought from the publisher, author or other copyright holder.

Versions of research

The version in the Kent Academic Repository may differ from the final published version.

Users are advised to check <http://kar.kent.ac.uk> for the status of the paper. **Users should always cite the published version of record.**

Enquiries

For any further enquiries regarding the licence status of this document, please contact:

researchsupport@kent.ac.uk

If you believe this document infringes copyright then please contact the KAR admin team with the take-down information provided at <http://kar.kent.ac.uk/contact.html>

Homo sapiens in Arabia by 85,000 years ago

Huw S. Groucutt^{1,2*}, Rainer Grün^{3,4}, Iyad S.A. Zalmout⁵, Nick A. Drake⁶, Simon J. Armitage^{7,8}, Ian Candy⁷, Richard Clark-Wilson⁷, Julien Louys³, Paul S. Breeze⁶, Mathieu Duval^{3,9}, Laura T. Buck^{10,11}, Tracy L. Kivell^{12,13}, Emma Pomeroy^{10,14}, Nicholas B. Stephens¹³, Jay T. Stock^{10,15}, Mathew Stewart¹⁶, Gilbert J. Price¹⁷, Leslie Kinsley⁴, Wing Wai Sung¹⁸, Abdullah Alsharekh¹⁹, Abdulaziz Al-Omari²⁰, Muhammad Zahir²¹, Abdullah M. Memesh⁵, Ammar J. Abdulshakoor⁵, Abdu M. Al-Masari⁵, Ahmed A. Bahameem⁵, Khaled S.M. Al Murayyi²⁰, Badr Zahrani²⁰, Eleanor M.L. Scerri^{1,2} & Michael D. Petraglia^{2,22*}

¹ School of Archaeology, Research Laboratory for Archaeology and the History of Art, Hayes House, 75 George Street, University of Oxford, Oxford, OX1 2BQ, UK.

² Department of Archaeology, Max Planck Institute for the Science of Human History, Kahlaische Stasse 10, D-07743, Jena, Germany.

³ Australian Research Centre for Human Evolution (ARCHE), Environmental Futures Research Institute, Griffith University, Nathan, QLD 4111, Australia.

⁴ Research School of Earth Sciences, The Australian National University, Canberra ACT, 0200, Australia.

⁵ Saudi Geological Survey, Sedimentary Rocks and Palaeontology Department, Jeddah 21514, Saudi Arabia.

⁶ Department of Geography, King's College London, Strand, London WC2R 2LS, UK

⁷ Department of Geography, Royal Holloway, University of London, TW20 0EX UK

⁸ SFF Centre for Early Sapiens Behaviour (SapienCE), University of Bergen, Post Box 7805, 5020, Bergen, Norway.

⁹ Geochronology, Centro Nacional de Investigación sobre la Evolución (CENIEH), Paseo Sierra de Atapuerca, 3, 09002 Burgos, Spain

- 27 ¹⁰PAVE Research Group, Dept. of Archaeology, University of Cambridge, Cambridge, CB2 3QG,
28 UK.
- 29 ¹¹Earth Sciences Department, Natural History Museum, Cromwell Road, London, SW7 5BD, UK.
- 30 ¹²Skeletal Biology Research Centre, School of Anthropology and Conservation, University of Kent,
31 Canterbury, CT2 7NR, UK.
- 32 ¹³Department of Human Evolution, Max Planck Institute for Evolutionary Anthropology, Deutscher
33 Platz 6, 04103, Leipzig, Germany.
- 34 ¹⁴School of Natural Sciences and Psychology, Liverpool John Moores University, Liverpool, L3 3AF,
35 UK.
- 36 ¹⁵Department of Anthropology, University of Western Ontario, London, Ontario, N6A 3K7, Canada.
- 37 ¹⁶Palaeontology, Geobiology and Earth Archives Research Centre, School of Biological, Earth and
38 Environmental Science, University of New South Wales, Sydney 2052, Australia.
- 39 ¹⁷School of Earth and Environmental Sciences, The University of Queensland, St Lucia 4072,
40 Queensland, Australia.
- 41 ¹⁸Department of Life Sciences, The Natural History Museum, Cromwell Road, London SW7 5BD,
42 UK.
- 43 ¹⁹Department of Archaeology, King Saud University, Riyadh, 12372 Saudi Arabia.
- 44 ²⁰Saudi Commission for Tourism and National Heritage, Riyadh 11586, Saudi Arabia.
- 45 ²¹Department of Archaeology, Hazara University, Mansehra, 21300, Pakistan.
- 46 ²²Human Origins Program, National Museum of Natural History, Smithsonian Institution,
47 Washington, DC, 20560, USA.

48

49 Corresponding authors: HSG (huw.groucutt@rlaha.ox.ac.uk) and MDP (petraglia@shh.mpg.de)

50

51

52

53 Understanding the timing and character of *Homo sapiens* expansion out of Africa is critical
54 for inferring the colonisation and admixture processes that underpin global population
55 history. It has been argued that dispersal out of Africa had an early phase, particularly ~130-
56 90 thousand years ago (ka), that only reached the East Mediterranean Levant, and a later
57 phase, ~60-50 ka, that extended across the diverse environments of Eurasia to Sahul.
58 However, recent findings from East Asia and Sahul challenge this model. Here we show that
59 *H. sapiens* was in the Arabian Peninsula before 85 ka. We describe the Al Wusta-1 (AW-1)
60 intermediate phalanx from the site of Al Wusta in the Nefud Desert, Saudi Arabia. AW-1 is
61 the oldest directly dated fossil of our species outside Africa and the Levant. The
62 palaeoenvironmental context of Al Wusta demonstrates that *H. sapiens* using Middle
63 Palaeolithic stone tools dispersed into Arabia during a phase of increased precipitation driven
64 by orbital forcing, in association with a primarily African fauna. A Bayesian model
65 incorporating independent chronometric age estimates indicates a chronology for Al Wusta of
66 ~95-86 ka, which we correlate with a humid episode in the later part of Marine Isotope Stage
67 5 known from various regional records. Al Wusta shows that early dispersals were more
68 spatially and temporally extensive than previously thought. Early *H. sapiens* dispersals out of
69 Africa were not limited to winter rainfall-fed Levantine Mediterranean woodlands
70 immediately adjacent to Africa, but extended deep into the semi-arid grasslands of Arabia,
71 facilitated by periods of enhanced monsoonal rainfall.

72

73 **Background**

74

75 *Homo sapiens* evolved in Africa in the late Middle Pleistocene¹. Early dispersals out of
76 Africa are evidenced at the Levantine site of Misliya at ~194-177 ka², followed by Skhul and
77 Qafzeh, where *H. sapiens* fossils have been dated to ~130-100 and ~100-90 ka respectively³.

78 While the Levantine fossil evidence has been viewed as the onset of a much broader dispersal
79 into Asia⁴⁻⁶, it has generally been seen as representing short-lived incursions into the
80 woodlands of the Levant immediately adjacent to Africa, where relatively high precipitation
81 is produced by winter storms tracking across the Mediterranean^{7,8}. While the Levantine
82 record indicates the subsequent local replacement of early *H. sapiens* by Neanderthals, the
83 failure of early dispersals to extend beyond the Levant is largely inferred from interpretations
84 of genetic data⁹. Genetic studies have suggested that recent non-African populations stem
85 largely¹⁰, if not entirely⁹, from an expansion ~60-50 ka, but this model remains debated. The
86 absence of low latitude Pleistocene human DNA and uncertainties regarding ancient
87 population structure undermine conclusions drawn from genetic studies alone. The paucity of
88 securely dated archaeological, palaeontological and ancient DNA data - particularly across
89 southern Asia - has made testing dispersal hypotheses challenging^{4,7,11}.

90
91 Recent fossil discoveries in East Asia indicate that the early (particularly Marine Isotope
92 Stage 5) dispersals of *Homo sapiens* extended across much of southern Asia. At Tam Pa Ling
93 in Laos, *Homo sapiens* fossils date to between 70 and 46 ka¹². Teeth assigned to *Homo*
94 *sapiens* from Lida Ajer cave, Sumatra, were recovered from a breccia dating to 68 ± 5 ka,
95 with fauna from the site dating to 75 ± 5 ka¹³. Several sites in China have produced fossil
96 material claimed to represent early *Homo sapiens*¹⁴. These include teeth from Fuyan Cave
97 argued to be older than 80 ka based on the dating of an overlying speleothem a few metres
98 from the fossils¹⁵, and teeth from Luna Cave that were found in a layer dating to between
99 129.9 ± 1.5 ka and 70.2 ± 1.4 ka¹⁶. Teeth and a mandible from Zhiren Cave, China, date to at
100 least 100 ka and have been argued to represent *Homo sapiens*, but other species attributions
101 are possible¹⁷. The recent documentation of a human presence in Australia from ~65 ka is
102 consistent with these findings¹⁸. Likewise, some interpretations of genetic data are consistent

103 with an early spread of *Homo sapiens* across southern Asia¹⁰. These discoveries are leading
104 to a radical revision of our understanding of the dispersal of *Homo sapiens*, yet there remain
105 stratigraphic and taxonomic uncertainties for many of the east Asian fossils^{14,19}, and
106 thousands of kilometers separate these findings from Africa.

107

108 The Arabian Peninsula is a vast landmass at the crossroads of Africa and Eurasia. Growing
109 archaeological evidence demonstrates repeated hominin occupations of Arabia^{20,21} each
110 associated with a strengthened summer monsoon which led to the re-activation of lakes and
111 rivers²²⁻²⁴, as it did in North Africa²⁵. Here we report the discovery of the first pre-Holocene
112 human fossil in Arabia, Al Wusta-1 (AW-1), as well as the age, stratigraphy, vertebrate
113 fossils and stone tools at the Al Wusta site (Fig. 1, see also Supplementary Information).

114

115 ***Figure 1 hereabouts***

116

117 **Results**

118 AW-1 is an intermediate manual phalanx, most likely from the 3rd ray (Fig. 2a,
119 Supplementary Information 1: see below for detail on siding and species identification). It is
120 generally well-preserved, although there is some erosion of the cortical/subchondral bone,
121 and minor pathological bone formation (likely an enthesophyte) affecting part of the
122 diaphysis (Supplementary Information 1). The phalanx measures 32.3 mm in proximo-distal
123 length, and 8.7 mm and 8.5mm in radio-ulnar breadth of the proximal base and midshaft,
124 respectively (Supplementary Table 1).

125

126 AW-1 is more gracile than the robust intermediate phalanges of Neanderthals²⁶⁻²⁸, which are
127 broader radio-ulnarly relative to their length and have a more 'flared' base. AW-1's proximal

128 radio-ulnar maximum breadth is 14.98 mm, which provides an intermediate phalanx breadth-
129 length index (proximal radio-ulnar maximum breadth relative to articular length) of 49.6.
130 This is very similar to the mean (\pm SD) for the Skhul and Qafzeh *H. sapiens* of 49.7 (\pm 4.1)
131 and 49.1 (\pm 4.0) for Upper Palaeolithic Europeans, but 1.89 standard deviations below the
132 Neanderthal mean of 58.3 (\pm 4.6)²⁹.

133

134 ***Figure 2 hereabouts***

135

136 To provide a broad interpretive context for the Al Wusta phalanx, we conducted linear and
137 geometric morphometric (GMM) landmark analyses (Supplementary Information 1) on
138 phalanges from non-human primates, fossil hominins and geographically widespread recent
139 *H. sapiens*. Comparative linear analyses (Supplementary Information 1, Supplementary
140 Tables 2 and 3, Supplementary Figure 1) reveal that there is substantial overlap across most
141 taxa for all shape ratios, so AW-1 falls within the range of variation of *H. sapiens*, cercopiths,
142 *Gorilla*, *Australopithecus afarensis*, *A. sediba* and Neanderthals. However, AW-1 is most
143 similar to the median value or falls within the range of variation of recent and early *H.*
144 *sapiens* for all shape ratios.

145

146 Geometric morphometric (GMM) analyses of AW-1 and various primate groups including
147 hominins (see Supplementary Table 4 and Supplementary Figure 2 for landmarks, and
148 Supplementary Table 5 for sample) are illustrated in Figure 3 and Supplementary Figure 3.
149 PC1 and PC2 together account for 61% of group variance in shape. AW-1 is separated on
150 these two shape vectors from the non-human primates and most of the Neanderthals. AW-1
151 falls closest to the recent and early *H. sapiens* and is clearly differentiated from all non-

152 human primates. This is also shown by the Procrustes distances from AW-1 to the mean
153 shapes of each taxonomic group (Supplementary Table 6).

154

155 ***Figure 3 hereabouts***

156

157 Three of the Neanderthal phalanges (from Kebara 2 and Tabun C1) are quite disparate from
158 the main Neanderthal cluster and fall closer to the *H. sapiens* and Al Wusta cluster on PC1
159 and 2 (Figure 3 and Supplementary Figure 3). Having established the hominin affinity of
160 AW-1, shape was analysed in more detail using a smaller hominin sample for which ray
161 number and side were known, which included Kebara 2 and Tabun C1. The broader primate
162 sample used in the first GMM analysis was not used for the more detailed shape analysis, as
163 the initial comparisons show clearly that AW-1 is not a non-human primate and including
164 this level of variation could potentially mask more subtle shape differences between
165 hominins. The side and ray are also not known for most of the Neanderthal and non-human
166 primate samples, meaning it would be impossible to evaluate the effect of these factors using
167 this sample.

168

169 The more in-depth shape comparison and modelling using the hominin sample of phalanges
170 of known ray and side (Supplementary Table 7) demonstrates that the long and slender
171 morphology of AW-1 falls just outside the range of variation of comparative Middle
172 Palaeolithic modern humans, but that its affinity is clearly with *H. sapiens* rather than
173 Neanderthals (Fig. 4, Supplementary Table 8). Although both Pleistocene *H. sapiens* and
174 Neanderthal landmark configurations fall almost completely inside the scatter for the
175 Holocene *H. sapiens* sample in the principal components analysis (Figure 4), AW-1 is closest
176 to Holocene *H. sapiens* 3rd intermediate phalanges. AW-1 overlaps with the Holocene *H.*

177 *sapiens* sample, but is separated from the Pleistocene *H. sapiens* specimens by a higher score
178 on PC2 and from the Neanderthal group by a simultaneously higher score on PC1 and PC2.
179 The Procrustes distances (Supplementary Table 8), also show that AW-1 is most distinct
180 from the Neanderthal phalanges, which fall towards the lower ends of both PCs and are
181 characterised by shorter and broader dimensions. PC1 and PC2 in this analysis show that
182 AW-1 is taller and narrower (in all directions: dorso-palmarly, proximo-distally and radio-
183 ulnarly) than almost all the phalanges in the comparative sample and is particularly distinct
184 from most of the Neanderthal phalanges. In this analysis AW-1 is closest in shape to 3rd
185 phalanges of individuals from (in descending order of proximity) Egyptian Nubia, and
186 Medieval Canterbury (UK), and Maiden Castle (Iron Age Dorset, UK) (Supplementary Table
187 9), although there is not a great difference in its distance to any of these specimens. These
188 analyses suggest that the AW-1 phalanx is likely to be a 3rd intermediate phalanx from a *H.*
189 *sapiens* individual.

190

191 ***Figure 4 hereabouts***

192

193 The third ray is the most symmetrical ray in the hand and is therefore difficult to side,
194 particularly when not all of the phalanges of a particular individual are present. Comparing
195 AW-1 separately to right and to left phalanges (Supplementary Information 1.4) gives results
196 which are very similar to the pooled sample, such that AW-1 is closest to Holocene *H.*
197 *sapiens* 3rd rays for both right and left hands (Supplementary Figure 4, Supplementary Table
198 10). There is little difference in morphological closeness between AW-1 and its nearest
199 neighbour in the samples of right and left bones (Supplementary Table 11), reflecting the lack
200 of difference in morphology between the sides. It is therefore not possible to suggest whether
201 AW-1 comes from a right or a left hand using these analyses.

202

203 AW-1 is unusual in its more circular midshaft cross-sectional shape (Fig. 2B), which is
204 confirmed by cross-sectional geometric analyses (Supplementary Information 1.5). This may
205 reflect the pronounced palmar median bar that makes the palmar surface slightly convex at
206 the midshaft rather than flat, the latter being typical of most later *Homo* intermediate
207 phalanges. However, more circular shafts may reflect greater loading of the bone in multiple
208 directions and enthesophytes are a common response to stress from high levels of physical
209 activity³⁰. This morphology may reflect high and varied loading of the fingers during intense
210 manual activity.

211

212 To determine the age of AW-1, and associated sediments and fossils, we used a combination
213 of uranium series (U-series), electron spin resonance (ESR) and optically stimulated
214 luminescence (OSL) dating (Methods, Supplementary Information 2 and 3). U-series ages
215 were produced for AW-1 itself (87.6 ± 2.5 ka) and hippopotamus dental tissues (WU1601),
216 which yielded ages of 83.5 ± 8.1 ka (enamel) and 65.0 ± 2.1 ka (dentine). They should be
217 regarded as minimum estimates for the age of the fossils. In addition, a combined U-series-
218 ESR age calculation for WU1601 yielded an age of $103 +10/-9$ ka. AW-1 was found on an
219 exposure of Unit 3b, and WU1601 excavated from Unit 3a, one metre away (Fig 1b). Unit 1
220 yielded OSL ages of 85.3 ± 5.6 ka (PD17), 92.2 ± 6.8 ka (PD41) and 92.0 ± 6.3 ka (PD15),
221 while Unit 3a yielded an OSL age of 98.6 ± 7.0 ka (PD40). The OSL age estimates agree
222 within error with the US-ESR age obtained for WU-1601 and the minimum age of ~ 88 ka
223 obtained for AW-1. These data were incorporated into a Bayesian sequential phase model³¹
224 which indicates that deposition of Unit 1 ceased 93.1 ± 2.6 ka (Phase 1: PD15, 17, 41) and
225 that Units 2 and 3 and all associated fossils were deposited between 92.2 ± 2.6 ka and $90.4 \pm$
226 3.9 ka (Phase 2: all other ages) (Supplementary Information 4, Supplementary Figure 11).

227

228 This ~95-86 ka timeframe is slightly earlier than most other records of increased humidity in
229 the region in late MIS 5^{32,33}, which correlate with a strengthened summer monsoon
230 associated with an insolation peak at 84 ka (Fig. 6). The underlying (Unit 3) aeolian sand
231 layer at Al Wusta correlates with an insolation minimum at the end of MIS 5c. The
232 chronometric age estimates for the site suggest that lake formation and the associated fauna
233 and human occupation occurred shortly after this in time. Regional indications of increased
234 humidity around the 84 ka insolation peak include speleothem formation at ~88 ka in the
235 Negev³⁴, and the formation of sapropel S3 beginning ~86 ka³⁵. In both the Levant and
236 Arabia, records are consistent with this switch from aridity to humidity around this time³²⁻⁴⁰.
237 Precisely reconstructing regional palaeoclimate at this time and relating it to human
238 demographic and behavioural change has proved challenging. This reflects both rapid
239 changes in climate, as well as the complexities involved in dating relevant deposits⁴¹. In
240 summary, combining chronological data (Supplementary sections 2-4), interpretation of the
241 sedimentary sequence (described below), and the regional setting of Al Wusta, we conclude
242 that lake formation and associated finds such as the AW-1 phalanx relate to the late MIS 5
243 humid period associated with the 84 ka insolation peak.

244

245 The sedimentary sequence at Al Wusta consists of a basin-like deposit of exposed carbonate-
246 rich sediments (Unit 2, 0.4-0.8 m thick), underlain by wind-blown sand (Unit 1) and overlain
247 by water-lain sands (Unit 3). The carbonate rich sediments of Unit 2 are interpreted as
248 lacustrine marl deposits on the basis of their sedimentology, geochemistry, and diatom
249 palaeoecology (Figure 1c, Methods, Supplementary Information 5). At both the macro- and
250 micro-scale, these beds are relatively massive and comprise fine-grained calcite, typical of
251 material precipitating and accumulating in a still-water lacustrine environment⁴². At the

252 micro-scale there is no evidence for the desiccation or fluctuation of water levels typical of
253 palustrine/wetland environments⁴², implying that the lake body was perennial. The diatom
254 flora support this, containing species such as *Aulacoseira italica* and *Aulacoseira granulata*
255 throughout the sequences, indicating an alkaline lake a few metres deep. The water was fresh,
256 not saline or brackish, since saline tolerant species and evaporitic minerals are absent
257 throughout. While $\delta^{18}\text{O}$ and $\delta^{13}\text{C}$ values of continental carbonates are controlled by a wide-
258 range of variables, the values derived from the Al Wusta marl beds are compatible with the
259 suggestion of marls precipitated in a perennial lake basin. The Al Wusta carbonate beds
260 therefore indicate a perennial lake body a few metres in depth. The existence of a marl
261 precipitating lake basin implies that this system was groundwater fed (to allow for sufficient
262 dissolved mineral material to be present in the lake waters). Although the Al Wusta sequence
263 represents a single lake basin, the development of such a feature over highly permeable
264 aeolian sands in a region where no lake systems exist at the present day implies a local
265 increase in water table that would require an increase in mean annual rainfall. Consequently,
266 the Al Wusta sequence represents the occurrence of a humid interval at this time. The Unit 2
267 marl is overlain by a medium-coarse sand (Unit 3) with crude horizontal laminations,
268 occasional clasts, fragments of ripped up marl and shells of *Melanoides tuberculata* and
269 *Planorbis* sp. While some vertebrate fossils and lithics were found in the upper part of Unit 2,
270 most were found in or on the surface of Unit 3. Unit 3a sands are waterlain and represent the
271 encroachment of fluvial sediment as the lake environment shallowed and contracted. Unit 3b
272 represents a winnowed lag formed by aeolian deflation of 3a. The sequence is capped by a
273 dense network of calcitic rhizoliths marking the onset of fully terrestrial conditions.
274
275 A total of 860 vertebrate fossils were excavated from Unit 3 and the top of Unit 2 (n=371)
276 and systematically surface collected (n=489). These include specimens attributed to Reptilia,

277 Aves, and Mammalia (Supplementary Table 19, Methods, Supplementary Information 6).
278 Notable taxa now extinct in Arabia are predominately grazers and include *Hippopotamus*,
279 *Pelorovis*, and *Kobus*. The faunal community demonstrates a clear preference for temperate
280 to semi-arid grasslands, and the presence of *Hippopotamus* and *Kobus* indicate permanent
281 muddy, fluvial, or lacustrine conditions⁴³ not currently found in the Nefud Desert, but
282 consistent with the geological evidence from the site. The faunal assemblages show a strong
283 affinity to African fauna, particularly *Hippopotamus*, *Pelorovis*, and *Kobus*⁴⁴. Many large
284 tooth pits on fossils indicate that large carnivores played a role in the accumulation of the
285 deposit. Long bone circumference, completeness and numbers of green fractures suggests
286 modification of bones by bone-breaking agents such as large carnivores or hominins
287 (Supplementary Information 6). However, no evidence of cut-marks or hammerstone damage
288 to the bones was observed.

289

290 An assemblage of 380 lithic artefacts (stone tools) was recovered from the excavation of
291 upper Unit 2 and Unit 3 and systematic surface collection (Methods, Figure 5, Supplementary
292 Information 7). They are of Middle Palaeolithic character and most are chert and quartzite.
293 The assemblage demonstrates a focus on centripetal Levallois reduction, and is similar to
294 other late Marine Isotope Stage 5 assemblages in the west and north of Arabia⁴⁵, and
295 contemporaneous assemblages in east (e.g. Aduma, BNS at Omo Kibish) and northeast
296 Africa (e.g. Bir Tarfawi), as well as those from the Levant (e.g. Qafzeh)¹¹ (Fig. 5).

297

298 ***Figure 5 hereabouts***

299 ***Figure 6 hereabouts***

300

301

302 **Discussion**

303

304 Al Wusta-1 is the oldest directly dated *H. sapiens* fossil outside Africa and the Levant. It
305 joins a small but growing corpus of evidence that the early dispersal of *H. sapiens* into
306 Eurasia was much more widespread than previously thought. The site of Al Wusta is located
307 in the Nefud desert more than 650 km southeast of Skhul and Qafzeh (Fig. 1A). This site
308 establishes that *H. sapiens* were in Arabia in late MIS 5, rather than being restricted to Africa
309 and the Levant as suggested by traditional models (Fig. 6). With Skhul dating to ~130-100
310 ka, Qafzeh to ~100-90 ka^{3,46} and Al Wusta to ~95-85 ka it is currently unclear if the
311 southwest Asian record reflects multiple early dispersals out of Africa or a long occupation
312 during MIS 5. The association of the Al Wusta site with a late MIS 5 humid phase (Fig. 6),
313 suggests that significant aspects of this dispersal process were facilitated by enhanced
314 monsoonal rainfall. While changes in behaviour and demography are crucial to understanding
315 the dispersal process, climatic windows of opportunity were also key in allowing *H. sapiens*
316 to cross the Saharo-Arabian arid belt, which often constituted a formidable barrier^{24,25}.

317

318 **Conclusion**

319

320 Al Wusta shows that the early, Marine Isotope Stage 5, dispersals of *H. sapiens* out of Africa
321 were not limited to the Levantine woodlands sustained by winter rainfall, but extended deep
322 into the Arabian interior where enhanced summer rainfall created semi-arid grasslands
323 containing abundant fauna and perennial lakes. After long being isolated in Africa^{1,47,48}, the
324 Late Pleistocene saw the expansion of our species out of Africa and into the diverse ecologies
325 of Eurasia. Within a few thousand years of spreading into Eurasia our species was occupying
326 rainforest environments and making long sea crossings to remote islands^{13,18}. Adapting to the

327 semi-arid conditions of the Saharo-Arabian arid belt represented a crucial step on this
328 pathway to global success and the Al Wusta *Homo sapiens* fossil demonstrates this early
329 ability to occupy diverse ecologies which led to us becoming a cosmopolitan species.

330

331 **References**

332

- 333 1. Stringer, C. The origin and evolution of *Homo sapiens*. *Philos. Trans. R. Soc. B. Biol.*
334 *Sci.* **371**, 20150237-20150237 (2016).
- 335 2. Hershkovitz, I., *et al.* The earliest modern humans outside Africa. *Science* **359**, 456-
336 459 (2018).
- 337 3. Grün, R. *et al.* U-series and ESR analyses of bones and teeth relating to the human
338 burials from Skhul. *J. Hum Evol.* **49**, 316-334 (2005).
- 339 4. Groucutt, H. S. *et al.* Rethinking the dispersal of *Homo sapiens* out of Africa. *Evol.*
340 *Anthropol.* **24**, 149-164 (2015).
- 341 5. Petraglia, M. D. *et al.* Middle Paleolithic assemblages from the Indian subcontinent
342 before and after the Toba super-eruption. *Science* **317**, 114-116 (2007).
- 343 6. Bae, C.J., Douka, K., Petraglia, M.D. On the origin of modern humans: Asian
344 perspectives. *Science* **358**, DOI: 10.1126/science.aai9067 (2017).
- 345 7. Mellars, P., Gori, K. C., Carr, M., Soares, P. A. & Richards, M. B. Genetic and
346 archaeological perspectives on the initial modern human colonization of southern
347 Asia. *Proc. Natl Acad. Sci. USA* **110**, 10699–10704 (2013).
- 348 8. Shea, J. J. Transitions or turnovers? Climatically-forced extinctions of *Homo sapiens*
349 and Neanderthals in the east Mediterranean Levant. *Quatern. Sci. Rev.* **27**, 2253-2270
350 (2008).

- 351 9. Mallick, S. *et al.* The Simons Genome Diversity Project: 300 genomes from 142
352 diverse populations. *Nature* **538**, 201-206 (2016).
- 353 10. Pagani, L. *et al.* Genomic analyses inform on migration events during the peopling of
354 Eurasia. *Nature* **538**, 238-242 (2016).
- 355 11. Groucutt, H. S. *et al.* Stone tool assemblages and models for the dispersal of *Homo*
356 *sapiens* out of Africa. *Quatern. Int.* **382**, 8-30 (2015).
- 357 12. Demeter, F., *et al.* Early Modern Humans from Tam Pà Ling, Laos. Fossil Review
358 and Perspectives. *Curr. Anthropol.* **57**, S17, DOI: 10.1086/694192 (2017)
- 359 13. Westaway, K.E., *et al.* An early modern human presence in Sumatra 73,000-63,000
360 years ago. *Nature* **548**, 322-325 (2017).
- 361 14. Michel, V., *et al.* The earliest modern *Homo sapiens* in China? *J. Hum. Evol.* **101**,
362 101-104 (2016).
- 363 15. Liu, W., *et al.* The early unequivocally modern humans in southern China? *Nature*
364 **526**, 696-699 (2015).
- 365 16. Bae, C., *et al.* Modern human teeth from Late Pleistocene Luna Cave (Guangxi,
366 China). *Quatern. Int.* **354**, 169-183 (2015).
- 367 17. Liu, W., *et al.* Human remains from Zhirendong, South China, and modern human
368 emergence in East Asia. *Proc. Natl. Acad. Sci. USA* **107**, 19201-19206 (2010).
- 369 18. Clarkson, C., *et al.* Human occupation of northern Australia by 65,000 years ago.
370 *Nature* **547**, 306-310 (2017).
- 371 19. Martínón-Torres, M., Wu, X., de Castro, J.M.B., Xing, S., Liu, W. *Homo sapiens* in
372 the Eastern Asian Late Pleistocene. *Curr. Anthropol.* **58**, S17, DOI: 10.1086/694449.
- 373 20. Groucutt, H. S. & Petraglia, M. D. The prehistory of Arabia: Deserts, dispersals and
374 demography. *Evol. Anthropol.* **21**, 113-125 (2012).

- 375 21. Petraglia, M. D., Groucutt, H. S., Parton, A. & Alsharekh, A., Green Arabia: Human
376 prehistory at the Cross-Roads of continents. *Quatern. Int.* **382**, 1-7 (2015).
- 377 22. Jennings, R. P. The greening of Arabia: Multiple opportunities for human occupation
378 in the Arabian Peninsula during the Late Pleistocene inferred from an ensemble of
379 climate model simulations. *Quatern. Int.* **205**, 181-199 (2015).
- 380 23. Rosenberg, T. M. *et al.* Middle and Late Pleistocene humid periods recorded in
381 palaeolake deposits in the Nafud desert, Saudi Arabia. *Quatern. Sci. Rev.* **70**, 109-123
382 (2013).
- 383 24. Breeze, P. S. *et al.* Palaeohydrological corridors for hominin dispersals in the Middle
384 East ~250-70,000 years ago. *Quatern. Sci. Rev.* **11**, 155-185 (2016).
- 385 25. Scerri, E. M. L., Drake, N. A., Jennings, R., Groucutt, H.S. Earliest evidence for the
386 structure of *Homo sapiens* populations in Africa. *Quatern. Sci. Rev.* **101**, 207-216
387 (2014).
- 388 26. Trinkaus, E. *The Shanidar Neandertals*. (Academic Press, New York, 1981).
- 389 27. McCown T. D. & Keith, A. *The Stone Age of Mount Carmel Volume 2: The fossil*
390 *human remains from the Levalloiso-Mousterian* (Clarendon Press, Oxford, 1939).
- 391 28. Vandermeersch, B. *Les hommes fossiles de Qafzeh (Israel)* (CNRS, Paris, 1981).
- 392 29. Walker, M. J., Ortega, J., López, M. V., Parmová, K. & Trinkaus, E. Neanderthal
393 postcranial remains from the Sima de las Palomas del Cabezo Gordo, Murcia,
394 Southeastern Spain. *Am. J. Phys. Anthropol.* **144**, 505-515 (2011).
- 395 30. Benjamin, M. *et al.* Where tendons and ligaments meet bone: attachment sites
396 ('entheses') in relation to exercise and/or mechanical load. *J. Anat.* **208**, 471-490.
- 397 31. Bronk Ramsey, C. Bayesian analysis of radiocarbon dates. *Radiocarbon* **51**, 337-360
398 (2009).

- 399 32. Drake, N. A., Breeze, P., Parker, A., 2013. Palaeoclimate in the Saharan and Arabian
400 Deserts during the Middle Palaeolithic and the potential for hominin dispersals.
401 *Quatern. Int.* **300**, 48-61 (2013).
- 402 33. Parton, A., et al. Orbital-scale climate variability in Arabia as a potential motor for
403 human dispersals. *Quatern. Int.* **382**, 82-97 (2015).
- 404 34. Vaks, A., Bar-Matthews, M., Matthews, A., Ayalon, A., Frumkin, A. Middle-Late
405 Quaternary paleoclimate of northern margins of the Saharan-Arabian Desert:
406 reconstruction from speleothems of Negev Desert, Israel. *Quatern. Sci. Rev.* **29**, 2647-
407 2662 (2010).
- 408 35. Grant, K.M., et al. The timing of Mediterranean sapropel deposition relative to
409 insolation, sea-level and African monsoon changes. *Quatern. Sci. Rev.* **140**, 125-141
410 (2016).
- 411 36. Bar-Matthews, M., Ayalon, A., Gilmour, M., Matthews, A. & Hawkesworth, C. J.
412 Sea-land oxygen isotopic relationships from planktonic foraminifera and speleothems
413 in the Eastern Mediterranean region and their implication for paleorainfall during
414 interglacial intervals. *Geochim. Cosmochim. Acta* **67**, 3181–3199 (2003).
- 415 37. Lisiecki, L. E. & Raymo, M. E. A Pliocene-Pleistocene stack of 57 globally
416 distributed benthic $\delta^{18}\text{O}$ records. *Paleoceanography* **20**, 1-17 (2005).
- 417 38. Berger, A. & Loutre, M. F. Insolation values for the climate of the last 10 million
418 years. *Quatern. Sci. Rev.* **10**, 297-317 (1991).
- 419 39. Fleitmann, D., Burns, S.J., Neff, U., Mangini, A., Matter, A. Changing moisture
420 sources over the last 333,000 years in Northern Oman from fluid-inclusion evidence
421 in speleothems. *Quatern. Res.* **60**, 223-232 (2003).
- 422 40. Rosenberg, T.M., et al. Humid periods in southern Arabia: Windows of opportunity
423 for modern human dispersal. *Geology* **39**, 1115-1118 (2011).

- 424 41. Clark-Balzan, L., Parton., A., Breeze, P.S., Groucutt, H.S., Petraglia, M.D. Resolving
425 problematic luminescence chronologies for carbonate- and evaporite-rich sediments
426 spanning multiple humid periods in the Jubbah Basin, Saudi Arabia. *Quatern.*
427 *Geochron.* <https://doi.org/10.1016/j.quageo.2017.06.002> (2018).
- 428 42. Alonso-Zarza, A. M. Palaeoenvironmental significant of palustrine carbonates and
429 calcretes in the geological record. *Earth Sci. Rev.* **60**, 261-298 (2003).
- 430 43. Estes, R. D. *The Behaviour Guide to African Mammals* (University of California
431 Press, Berkeley, 1991).
- 432 44. O'Regan, H. J., Turner, A., Bishop, L. C., Elton, S., Lamb, A. L. Hominins without
433 fellow travellers? First appearances and inferred dispersals of Afro-Eurasian large-
434 mammals in the Plio-Pleistocene. *Quatern. Sci. Rev.* **30**, 1343-1352 (2011).
- 435 45. Groucutt, H.S. et al. Human occupation of the Arabian Empty Quarter during MIS 5:
436 evidence from Mundafan al-Buhayrah. *Quatern. Sci. Rev.* **119**, 116-135 (2015).
- 437 46. Millard, A. R. A critique of the chronometric evidence for hominid fossils: I. Africa
438 and the Near East 500-50 ka. *J. Hum. Evol.* **54**, 848-874 (2008).
- 439 47. Hublin, J.J., et al. New fossils from Jebel Irhoud, Morocco and the pan-African origin
440 of *Homo sapiens*. *Nature* **546**, 289-292 (2017).
- 441 48. Richter, D., et al. The age of the hominin fossils from Jebel Irhoud, Morocco, and the
442 origins of the Middle Stone Age. *Nature* **546**, 293-296 (2017).

443

444

445

446

447

448

449 **Supplementary Information** is available in the online version of the paper.

450

451 **Acknowledgements.** We thank HRH Prince Sultan bin Salman bin Abdulaziz Al-Saud,
452 President of the Saudi Commission for Tourism and National Heritage (SCTH), and Prof. Ali
453 Ghabban, Vice President of the SCTH for permission to carry out this study. Dr Zohair
454 Nawab, President of the Saudi Geological Survey, provided research support and logistics.
455 Fieldwork and analyses were funded by the European Research Council (no. 295719, to MDP
456 and 617627, to JTS), the SCTH, the British Academy (HSG and EMLS), The Leverhulme
457 Trust, the Australian Research Council (DP110101415 to RG, FT150100215 and
458 TF15010025 to MD, and FT160100450 to JL), and the Research Council of Norway (SFF
459 Centre for Early Sapiens Behaviour, 262618). We thank Patrick Cuthbertson, Klint Janulis,
460 Marco Bernal, Salih Al-Soubhi, Mohamad Haptari, Adel Matari, and Yahya Al-Mufarreh for
461 assistance in the field. We thank Ian Cartwright (Institute of Archaeology, University of
462 Oxford) for the photographs of AW-1 (Fig. 2a), Ian Matthews (RHUL) for producing the
463 Bayesian age model, and Michelle O'Reilly (MPI-SHH) for assistance with the preparation
464 of figures. We acknowledge the Max Planck Society for supporting us with comparative
465 fossil data, and we thank curators for access to comparative extant and fossil material in their
466 care (Supplementary Tables 5 and 7).

467

468 **Author Contributions** H.S.G. and M.D.P. designed, coordinated and supervised the study.
469 H.S.G., I.S.Z., N.D, S.A., I.C., R.C-W., J.L., P.S.B., M.S., G.J.P., A.A., A.A.-O., A.M. B.A.,
470 E.M.L.S. and M.D.P. conducted excavation, survey and multidisciplinary sampling at Al
471 Wusta. L.T.B., T.L.K., E.P., N.B.S and J.T.S. conducted the morphological analysis and
472 comparative study of the AW-1 phalanx. R.G., M.D. and L.K. carried out the U-series and
473 ESR analyses. S.J.A. and R.C.W carried out the OSL dating. I.C. and R.C.W conducted the

474 stratigraphic and sedimentological analysis of the site, with input from N.D., J.L. and G.J.P.
475 W.W.S. analysed the diatoms. M.S. and J.L. analysed the vertebrate fossils, with input from
476 G.J.P. Lithic analysis was conducted by H.S.G. and E.M.L.S. Spatial analyses were
477 conducted by P.S.B. All authors helped to write the paper.

478

479 **Author Information** The authors declare no competing financial interests.

480 Readers are welcome to comment on the online version of the paper.

481 Correspondence and requests for materials should be addressed to

482 H.S.G. (huw.groucutt@rlaha.ox.ac.uk) or M.D.P. (petraglia@shh.mpg.de).

483

484 **Data availability statement.** Authors can confirm that all relevant data are included in the
485 paper and/ or its supplementary information files.

486

487

488

489

490

491

492

493

494

495

496

497

498

499

500 **Figure captions**

501

502 **Figure 1. Al Wusta location, map of site and stratigraphy.** A: The location of Al Wusta
503 and other key MIS 5 sites in the region¹¹; B: Al Wusta digital elevation model showing
504 location of AW-1 phalanx, marl beds, lithics and vertebrate fossils, and the locations of the
505 trenches and sections. The inset shows a satellite image of the site; C: Stratigraphic log of Al
506 Wusta showing the sedimentology of the exposed carbonate beds, isotopic values, OSL ages
507 for sand beds and U-series and ESR ages for AW-1 and WU-1601. Sands are shown in
508 yellow: lower massive sands are aeolian (Unit 1), upper laminated sands are waterlain (Unit
509 3a) and have been locally winnowed to generate a coarse desert pavement (Unit 3b),
510 lacustrine marls are shown (Unit 2) in grey (for full key and description see Supplementary
511 Figures 13 and 14 and Supplementary Information 5). Section PD40 is shown as it contains
512 the thickest sequence and is most representative of Al Wusta, chronometric age estimates
513 (marked *) from the site are depicted in their relative stratigraphic position, see
514 Supplementary Figure 14 for their absolute positions.

515

516 **Figure 2. Photographs and micro-CT scans of Al Wusta-1 *Homo sapiens* phalanx.** A:
517 photographs in (left column, top to bottom) distal, palmar and proximal views, and (middle
518 row, left to right) lateral 1, dorsal and lateral 2 views. Micro-CT cross-sections (illustrated at
519 2x magnification) include B (54% from proximal end) and C (illustrating abnormal bone).

520

521 **Figure 3. Scatterplot of the first two principal components (PC) scores of the geometric**
522 **morphometric analysis of the Al Wusta-1 phalanx compared with a sample of primates,**
523 **including hominins.** Non-human hominoids: lilac; *Gorilla*: circles, *Pan*: triangles.

524 Cercopithecoids: red; *Colobus*: triangles, *Mandrillus*: squares, *Papio*: circles. Neanderthals:
525 blue diamonds. *H. sapiens*: green; early *H. sapiens*: circles, Holocene *H. sapiens*: squares. Al
526 Wusta-1: black star, circled in red.

527

528 **Figure 4: Scatterplot of the first two principal component (PC) scores from the**
529 **geometric morphometric analyses of AW-1 and sample of comparative hominin 2nd, 3rd,**
530 **and 4th intermediate phalanges.** Wireframes show mean configuration warped to extremes
531 of PC axes in dorsal (left), proximal (middle) and lateral (right) views. Convex hulls added
532 post-hoc to aid visualisation.

533

534 **Figure 5. Selected Al Wusta lithic artefacts.** A: argillaceous quartzite flake; B: quartz
535 hammerstone; C: ferruginous quartzite Levallois flake; D: chert Levallois flake; E: Quartz
536 recurrent centripetal Levallois core; F: quartzite preferential Levallois core with centripetal
537 preparation and pointed preferential removal.

538

539 **Figure 6. The chronological and climatic context of Al Wusta.** The Al Wusta lake phase
540 falls chronologically at the end of the time-range of MIS 5 sites from the Mediterranean
541 woodland of the Levant (~130-90 ka) and earlier than the late dispersal(s) (~60-50 ka) as
542 posited in particular by genetic studies. The chronology of these dispersals and occupations
543 correspond with periods of orbitally modulated humid phases in the eastern Mediterranean³⁶
544 that are important intervals for human dispersals into Eurasia, and are also proposed to
545 correspond with episodes of monsoon driven humidity in the Negev and Arabian desert³⁴.
546 Environmental amelioration of the Saharo-Arabian belt, therefore, appears to be crucial for
547 allowing occupation at key sites that document dispersal out of Africa. A: East Mediterranean
548 speleothem $\delta^{18}\text{O}$ record from Soreq and Pequin Caves³⁶; B: global $\delta^{18}\text{O}$ record³⁷; C:

549 Insolation at 30 degrees north³⁸, showing the temporal position of key sites relating to
550 dispersal out of Africa^{2,3,11,48}. The chronology for Al Wusta shows the phases defined by the
551 Bayesian model at 2σ .

552

553

554

555

556

557

558

559

560

561

562

563

564

565

566

567

568

569

570

571

572

573

574

575 **Methods**

576

577 **Site identification, survey and excavation.** The site of Al Wusta (field code WNEF16_30)
578 was discovered in 2014 as part of a programme of joint survey fieldwork of the Palaeodeserts
579 Project, the Saudi Commission for Tourism and National Heritage, and the Saudi Geological
580 Survey. It is located in the western Nefud desert, a few kilometres from the Middle
581 Pleistocene fossil locality of Ti's al Ghaddah⁴⁹. The locations of all materials of interest
582 (fossils, stone tools, geomorphological features, excavations and sample points) were
583 recorded using a high-precision Trimble XRS Pro Differential GPS system and a total station,
584 and entered into a GIS (Fig. 1). Elevation data (masl) were recorded as a series of transects
585 across the site, and a digital elevation model (DEM) and contours interpolated (Spline) from
586 all data with precisions of better than 10 cm in all (x,y,z) dimensions (22,047 points). This
587 allowed visualisation and recording of the spatial relationships between materials in three
588 dimensions (Fig. 1). Eight trenches were excavated into the fossil and artefact bearing
589 deposits. These trenches revealed vertebrate remains and lithics, but no further human fossils
590 were recovered.

591

592 **Morphological analysis of Al Wusta-1 phalanx.** The phalanx was scanned using micro-
593 computed tomography (micro-CT) on the Nikon Metrology XT H 225 ST High Resolution
594 scanner and X-Tek software (Nikon Metrology, Tring, UK) housed in the Cambridge
595 Biotomography Centre, University of Cambridge, UK. Scan parameters were: a tungsten
596 target; 0.5 mm copper filter; 150 kV; 210 mA; 1080 projections with 1000 ms exposure, and
597 resulted in a voxel size of 0.02 mm³. The micro-CT data were reconstructed using CT-PRO
598 3D software (Nikon Metrology) and exported as an image (.tif) stack. Other CT data were

599 obtained from the institutions cited in Supplementary Table 5 with permissions following the
600 memoranda of understanding with each institution.

601

602 3D landmarks and semilandmarks were chosen to best describe the overall shape of the
603 morphology of the AW-1 phalanx (Supplementary Table 4, Supplementary Figure 2), and
604 were digitised on virtual reconstructions of phalanges created from micro-CT data in AVIZO
605 8 and 9.1 (FEI Software, Burlington, Mass.). Landmark coordinates were exported for use in
606 Morphologika⁵⁰. In Morphologika, generalized Procrustes analyses were performed to
607 superimpose landmark coordinate data, and principal components analyses (PCA) were run
608 to investigate similarities in shape between specimens. Shape differences along principal
609 componentss were visualised and wireframes were produced in Morphologika, PC scores
610 were exported to create graphs in R⁵¹. Procrustes distances between specimens were
611 calculated using MorphoJ⁵². To avoid representing the same phalanges from different sides of
612 a single individual as independent data points and to maximise sample sizes in pooled
613 analyses, right phalanges were used in cases where the phalanges from both sides were
614 present. Where only the left was present, this was used and ‘reflected’ (i.e. mirrored) in
615 Morphologika to generate landmark configurations consistent with right phalanges.

616

617 **U-series and combined US-ESR dating of fossil bone and teeth.** The AW-1 phalanx (lab
618 number 3675) and a hippopotamus tooth fragment (lab number WU1601) were collected
619 from Trench 1 (Fig.1) for U-series and combined US-ESR dating, respectively. The external
620 dose rate utilised the data of OSL sample PD40, which was collected in an equivalent
621 position within unit 3a.

622

623 *U-series analysis.* U-series analyses were conducted at the Research School of Earth
624 Sciences, The Australian National University, Canberra. The experimental setup for the U-
625 series analysis of the phalanx was described in detail by Grün and colleagues⁵³
626 (Supplementary Figures 2 and 3, Supplementary Information 2). Laser ablation (LA) was
627 used to drill a number of holes into AW-1 following the approach of Benson and
628 colleagues⁵⁴. After a cleaning run with the laser set at a diameter of 460 µm, seven holes were
629 drilled for 1000 s with the laser set at 330 µm. The isotopic data streams were converted into
630 $^{230}\text{Th}/^{234}\text{U}$ and $^{234}\text{U}/^{238}\text{U}$ activity ratios and apparent Th/U age estimates and subsequently
631 binned into 30 successive sections (each containing 33 cycles) for the calculation of average
632 isotopic ratios and ages. A similar experimental setup and methodology were employed for
633 the LA U-series analysis of tooth sample WU1601. The whole closed system U-series
634 analytical datasets of the enamel and dentine sections were integrated to provide the data
635 input for the ESR age calculations.

636

637 *Combined US-ESR dating of the fossil tooth: ESR dose evaluation.* The ESR dose evaluation
638 of the hippo tooth was carried out at CENIEH, Burgos, Spain, following a similar procedure
639 to that described in Stimpson and colleagues⁴⁹. Enamel was collected from WU1601 and
640 powdered <200 µm. The sample was then divided into 11 aliquots and gamma irradiated with
641 a Gammacell-1000 Cs-137 source to increasing doses until 3.4 kGy. ESR measurements were
642 carried out at room temperature with an EMXmicro 6/1 Bruker ESR spectrometer coupled to
643 a standard rectangular ER 4102ST cavity. ESR intensities were extracted from T1-B2 peak-
644 to-peak amplitudes of the ESR signal of enamel. Fitting procedures were carried out with a
645 single saturating exponential (SSE) function through the pooled ESR experimental data
646 derived from the repeated measurements, with data weighting by the inverse of the squared
647 ESR intensity ($1/I^2$) and following the recommendations by Duval and Grün⁵⁵. Full details

648 about the experimental conditions and analytical procedure may be found in Supplementary
649 Information 2.

650

651 *Combined US-ESR dating of the fossil tooth: Dose rate evaluation and age calculations.* The
652 combined US-ESR age of WU1601 was calculated with the DATA programme⁵⁶ using the
653 US model defined by Grün and colleagues⁵⁷. The following parameters were used for the
654 dose rate evaluation: an alpha efficiency of 0.13 ± 0.02 ⁵⁸, Monte-Carlo beta attenuation
655 factors from Marsh⁵⁹, dose-rate conversion factors from Guerin and colleagues⁶⁰, external
656 sediment (beta and gamma) dose rate from the OSL sample PD40, a depth of 25 ± 10 cm,
657 resulting in an age of $103 + 10/-9$ ka.

658

659 **Optically Stimulated Luminescence Dating.** Three samples (PD15, PD17 and PD41) were
660 collected from the aeolian sands (Unit 1) underlying the southern marl outcrop (Unit 2, Fig
661 1B). A fourth sample (PD40) was taken from the main fossil bearing bed (Unit 3). Individual
662 quartz grains were measured on a Risø TL/OSL-DA-15 instrument using the single-aliquot
663 regenerative-dose (SAR) method⁶¹. The burial dose for each sample (D_b) was calculated
664 using the central age model (CAM)⁶².

665

666 Environmental dose rates were determined using a Risø GM-25-5 low-level beta counting
667 system⁶³ (beta dose rate), field gamma spectrometry (gamma dose rate), and an estimate of
668 the cosmic dose rate derived using site location and present day sediment burial depths⁶⁴. Full
669 optically stimulated luminescence dating methods and results are presented in Supplementary
670 Information Section 3. All analyses were carried out in the Royal Holloway Luminescence
671 Laboratory by SA and R C-W.

672

673 **Age modelling.** Chronometric ages for samples from the Al Wusta site were incorporated
674 into a Bayesian sequential phase model implemented in OxCal v4.2³¹ (Supplementary
675 Information 4; Supplementary Figure 11. The model consists of two discrete phases separated
676 by a hiatus. Phase 1 was defined by the three OSL ages (PD15, 17 and 41) for samples from
677 the aeolian sands (Unit 1) underlying the lacustrine marls (Unit 2). Phase 2 was defined by
678 the ages for the sand (PD40) and fossils (AW-1 and WU1601) from the waterlain sediments
679 (Unit 3) overlying Unit 2. U-series ages for WU1601 and AW-1 were treated as minimum
680 age estimates, whereas PD40 and the combined U-series-ESR age on WU1601 were treated
681 as finite age estimates. Since the Al Wusta sequence accumulated over a short period of time,
682 and contains only five finite ages (and three minimum ages), the General Outlier Model³¹ was
683 unable to function, and instead a simpler model using agreement indices was employed. This
684 analysis yielded Amodel (76) and Aoverall (79) values well in excess of the generally
685 accepted threshold (60³¹), with only one age yielding an individual agreement index below
686 this threshold (PD17, 51). These data indicate that no ages should be excluded from the
687 model, and that the age model itself is robust. The Bayesian sequential model yielded an age
688 for the end of Phase 1 of 93.1 ± 2.6 ka (1 σ uncertainties), while Phase 2 yielded start and end
689 dates of 92.2 ± 2.6 ka and 90.4 ± 3.9 ka respectively. The end date for phase 2 should be
690 treated as a maximum value since no overlying material is present, precluding the possibility
691 of further constraining the end of this phase.

692

693 **Stratigraphy and sedimentology.**

694 *Sediment analysis.* Bulk samples (in the form of coherent blocks) were taken at 10 cm
695 intervals through each of the marl beds in four sections (Fig. 1C and Supplementary Figures
696 13 and 14). Each block was air-dried and subsamples (ca 0.5 g) were removed, powdered and
697 analysed for percentage carbonate content using Bascomb calcimetry, which measures the

698 volume of carbon dioxide liberated from a known sample mass during reaction with 10%
699 HCl⁶⁵. Thin sections were prepared from fresh sediment blocks. The sediments did not
700 require acetone treatment as they were already dry and, due to their permeability, were
701 impregnated with a bonding resin. Standard thin section preparation was then carried out
702 using techniques developed in the Centre for Micromorphology at Royal Holloway,
703 University of London⁶⁶. Thin sections were analysed using an Olympus BX-50 microscope
704 with magnifications from 20x to 200x and photomicrographs were captured with a Pixera
705 Penguin 600es camera. A point-count approach was used to produce semi-quantified data
706 from the thin sections, based on counting micro-features at 3 mm intervals along linear
707 transects 1 cm apart. Kemp⁶⁷, Stoops⁶⁸ and Alonso-Zarza⁴² were referred to when identifying
708 features. X-ray diffraction analysis (XRD) was carried out in the Department of Earth
709 Sciences (Royal Holloway, University of London). Powdered samples were analysed on a
710 Philips PW1830/3020 spectrometer with copper K α X-rays. Mineral peaks were identified
711 manually from the ICDD Powder Diffraction File (PDF) database. The methods and results
712 are described further in Supplementary Information 5.

713

714 *Diatoms.*

715 *Sample preparation.* Samples were analysed using the standard method of Renberg⁶⁹
716 (Supplementary Information 5). Thus, all samples were treated with 30% H₂O₂ and 5% HCl
717 to digest organic material and remove calcium carbonate. Distilled water was added to dilute
718 the samples after heating, which were then stored in the refrigerator for four days to minimise
719 further chemical reactions. The samples were rinsed daily and allowed to settle overnight. A
720 known volume of microspheres was added to the supernatant after the last rinse to enable
721 calculation of the diatom concentration⁷⁰. The slides were air-dried at room temperature in a
722 dust free environment before mounting with Naphrax diatom mountant. Diatom taxonomy

723 followed Krammer and Lange-Bertalot⁷¹⁻⁷³ and taxonomic revisions^{74,75} with at least 300
724 valves enumerated for a representative sample at x1000 magnification.
725
726 *Numerical analysis.* Prevalent trends in the diatom assemblage were explored using
727 ordination analyses using CANOCO 4.5 of ter Braak and Šmilauer⁷⁶. Detrended
728 Correspondence Analysis (DCA⁷⁷) with detrending by segments and down-weighting of rare
729 species was used to investigate taxonomic variations within each site and to determine
730 whether linear or unimodal models should be used for further analyses. If the gradient length
731 of the first axis is <1.5 SD units, linear methods (Principle Component Analysis, PCA)
732 should be used; however, if the gradient length is >1.5 SD units, unimodal methods
733 (Correspondence Analysis) should be used⁷⁸. Detrended Canonical Correspondence Analysis
734 (DCCA⁷⁹) was also used to show changes in compositional turnover scaled in SD units.
735 Therefore, variations in the down-core DCCA first axis sample scores show an estimate of
736 the compositional change between samples along an environmental or temporal gradient.
737 Depth was used as the sole constraint as the samples in each site are in a known temporal
738 order⁸⁰. The dataset was square-root transformed to normalise the distribution prior to
739 analyses. Optimal sum-of-squares partitioning⁸¹ with the program ZONE⁸² and comparison of
740 the zones with the Broken-stick model using the program BSTICK⁸³ were used to determine
741 significant zones. The planktonic: benthic ratio, habitat summary, concentration and the F
742 index (a dissolution index⁸⁴) were calculated for all the samples.

743

744 *Stable isotopes*

745 It is common practice, when analysing the $\delta^{18}\text{O}$ and $\delta^{13}\text{C}$ values of lacustrine/palustrine
746 carbonates to either: 1) sieve the sediment and analyse the <63 μm fraction, or 2) use the
747 microstructure of the sample, as identified under thin section, to identify pure, unaltered

748 fabrics, which can then be drilled out and analysed⁸⁵. The former procedure ensures that the
749 analysed fraction comprises pure authigenic marl (rather than a mixture of ostracod,
750 mollusc, chara and marl components that will contain different isotopic values). The latter is
751 done to ensure that any carbonate that has been affected by diagenesis is sampled. Neither of
752 these approaches were carried out here as; 1) microfabric analysis showed no evidence for
753 diagenesis (although some of the samples are cemented the cement makes a negligible
754 component of sample mass), and 2) some of the samples have incipient cementation, which
755 means that they cannot be sieved. Bulk carbonate powders were consequently analysed for
756 $\delta^{18}\text{O}$ and $\delta^{13}\text{C}$. To show that the analysis of bulk samples had no impact on the derived
757 isotopic data, samples that were friable enough to be sieved were treated with sodium
758 hexametaphosphate to disaggregate them and then homogenised and separated into two
759 subsamples for isotopic analysis; (1) a sieved $<63\mu\text{m}$ fraction and (2) a homogenised bulk
760 sample. The resulting isotopic data showed no difference between the $\delta^{18}\text{O}$ and $\delta^{13}\text{C}$ values
761 of the sieved and bulk samples (Supplementary Figure 13b), highlighting that the
762 homogenous and unaltered nature of the material results in bulk carbonate isotopic analysis
763 generating valid data. Two samples were taken from different locations of each sampled
764 block to generate a larger dataset of independent samples. The $\delta^{18}\text{O}$ and $\delta^{13}\text{C}$ values of each
765 samples were determined by analysing CO_2 liberated from the reaction of the sample with
766 phosphoric acid at 90°C using a VG PRISM series 2 mass spectrometer in the Earth Sciences
767 Department at Royal Holloway. Internal (RHBNC) and external (NBS19, LSVEC) standards
768 were run every 4 and 18 samples respectively. 1σ uncertainties are 0.04‰ ($\delta^{18}\text{O}$) and 0.02‰
769 ($\delta^{13}\text{C}$). All isotope data presented in this study are quoted against the Vienna Pee Dee
770 Belemnite (VPDB) standard.

771

772 **Vertebrate fossil analyses.** Each fossil specimen was identified to lowest taxonomic and
773 anatomical level possible (Supplementary Figure 20, Supplementary Table 19 and
774 Supplementary Information 6). Taxonomic identification and skeletal element portions were
775 determined based on anatomical landmarks, and facilitated by comparisons with the
776 Australian National University Archaeology and Natural History reference collection
777 (Canberra), unregistered biological collections held at the University of New South Wales
778 (Sydney), and the large mammal collections of the Zoologische Staatssammlung München
779 (Munich). Each specimen was assigned a size category (small, medium, and large) following
780 Dominguez-Rodrigo and colleagues⁸⁶, and corresponding to the five size classes described in
781 Bunn⁸⁷, where small, medium and large denote size classes 1-2, 3A-3B and 4-6, respectively.
782 Element abundance is reported as Number of Identified Specimens (NISP).

783

784 Each specimen was examined for modification by eye and hand-lens (10x) under both natural
785 and high-incidence light, and examined at different angles to assist identification of fine-scale
786 surface modifications. Where required, further examination and photography was carried out
787 using a digital microscope (Model: Dino-lite, AM7013MZ). Morphometric data (length,
788 breadth and width) was measured using digital callipers (Model: Mitutoyo Corp, CD-
789 8"PMX), and specimen weights using a digital scale. Bone surface modifications were
790 identified and recorded following standard methodologies: butchery and tooth marks⁸⁸⁻⁹⁴,
791 burning⁹⁵⁻⁹⁶, rodent gnawing^{97,98}, weathering⁹⁹ and trampling¹⁰⁰. Carnivore damage was
792 categorized as pit, score, furrow or puncture, and the location noted⁹⁴. Tooth mark
793 morphometric data – short and long axes – was also recorded. Any additional modifications,
794 i.e. polish, manganese staining, and root etching, were also reported and described. Bone
795 breakage was recorded as green, dry, or both, following Villa and Mahieu¹⁰¹. Long bone

796 circumference completeness was recorded using the three categories described by Bunn¹⁰²:
797 type 1 (<1/2), type 2 (>1/2 but < complete) and type 3 (complete).

798

799 **Lithic analysis.** Lithics were systematically collected during pedestrian transects and
800 excavations of Al Wusta. This produced a total studied assemblage of 380 lithics
801 (Supplementary Information 7). Further lithics extended for a considerable distance to the
802 north, seeming to track the outlines of the palaeolake, but we only conducted detailed
803 analysis on lithics from the southern part of the site, close to AW-1 and the sedimentary ridge
804 on which it was found (i.e. south of the Holocene playa). These were analysed using the
805 methodology described in Scerri and colleagues^{25,103,104} and Groucutt and colleagues^{45,105}. As
806 well as qualitative analysis of technological features indicating particular techniques and
807 methods of reduction, a variety of quantitative features such as dimensions, the number of
808 scars and % of cortex were recorded. Informative examples were selected for photography
809 and illustration. This approach allows both a characterisation and description of the
810 assemblage and broad comparison with other assemblages from surrounding regions.

811

812

813

814

815

816

817

818

819

820

821 **Methods References**

822

823 49. Stimpson, C. et al. Middle Pleistocene vertebrate fossils from the Nefud Desert, Saudi
824 Arabia: Implications for biogeography and palaeoecology. *Quatern. Sci. Rev.* **143**, 13-
825 36 (2016).

826 50. O'Higgins, P., Jones, N. Facial growth in *Cercocebus torquatus*: an application of
827 three-dimensional geometric morphometric techniques to the study of morphological
828 variation. *J. Anat.* **193**, 251-72 (1998).

829 51. R Core Team. *R: A Language and Environment for Statistical Computing*. (Vienna,
830 Austria: R Foundation for Statistical Computing, <http://www.R-project.org>, 2015).

831 52. Klingenberg C, P. MorphoJ: an integrated software package for geometric
832 morphometrics. *Mol. Ecol. Resour.* **11**, 353-7 (2011)

833 53. Grün, R., Eggins, S., Kinsley, L., Mosely, H., Sambridge, M. Laser ablation U-series
834 analysis of fossil bones and teeth. *Palaeogeogr., Palaeoclimatol., Palaeoecol.* **416**,
835 150-167 (2014).

836 54. Benson, A., Kinsley, L., Defleur, A., Kokkonen, H., Mussi, M., Grün, R. Laser
837 ablation depth profiling of U-series and Sr isotopes in human fossils. *J. Arch. Sci.* **40**,
838 2991-3000 (2013).

839 55. Duval, M., Grün, R. Are published ESR dose assessments on fossil tooth enamel
840 reliable? *Quat. Geochron.* **31**, 19-27 (2016).

841 56. Grün, R. The DATA program for the calculation of ESR age estimates on tooth
842 enamel. *Quatern. Geochron.* **4**, 231-232 (2009).

843 57. Grün, R., Schwarcz, H.P., Chadam, J. ESR dating of tooth enamel: Coupled
844 correction for U-uptake and U-series disequilibrium. *Int. J. Radiat. Appl. Instrum.*
845 *Nucl. Tracks. Radiat. Meas.* **14**, 237-241 (1988).

- 846 58. Grün, R., Katzenberger-Apel, O. An alpha irradiator for ESR dating. *Ancient TL* **12**,
847 35-38 (1994).
- 848 59. Marsh, R. E. Beta-gradient Isochrons Using Electron Paramagnetic Resonance:
849 Towards a New Dating Method in Archaeology. (MSc thesis, McMaster University,
850 Hamilton, 1999).
- 851 60. Guérin, G., N. Mercier and G. Adamiec. Dose-rate conversion factors: update.
852 *Ancient TL* 29(1): 5-8 (2011).
- 853 61. Murray, A. S., Wintle, A. G. Luminescence dating of quartz using an improved
854 single-aliquot regenerative-dose protocol. *Radiat. Meas.* **32**, 57-73 (2000).
- 855 62. Galbraith, R. F., Roberts, R. G., Laslett, G. M., Yoshida, H., Olley, J. M. Optical
856 dating of single and multiple grains of quartz from Jinmium rock shelter, northern
857 Australia: Part I, experimental design and statistical models. *Archaeometry* **41**, 339-
858 364 (1999).
- 859 63. Bøtter-Jensen, L., Mejdahl, V. Assessment of beta dose-rate using a GM multicounter
860 system. *Int. J. Rad. Appl. Instrum. B.* **14**, 187-191 (1988).
- 861 64. Prescott, J. R., Hutton, J. T. Cosmic ray and gamma ray dosimetry for TL and ESR.
862 *Int. J. Rad. Appl. Instrum.* **14**, 223-227 (1988).
- 863 65. Gale, S., Hoare, P. *Quaternary Sediments: Petrographic Methods for the Study of*
864 *Unlithified Rocks* (Belhaven and Halsted Press, 1991).
- 865 66. Palmer, A. P., Lee, J. A., Kemp, R. A., Carr, S. J. *Revised laboratory procedures for*
866 *the preparation of thin sections from unconsolidated sediments*. (Centre for
867 micromorphology publication, Royal Holloway, University of London, 2008).
- 868 67. Kemp, R. A. *Soil micromorphology and the Quaternary*. (Quaternary Research
869 Association, 1985).

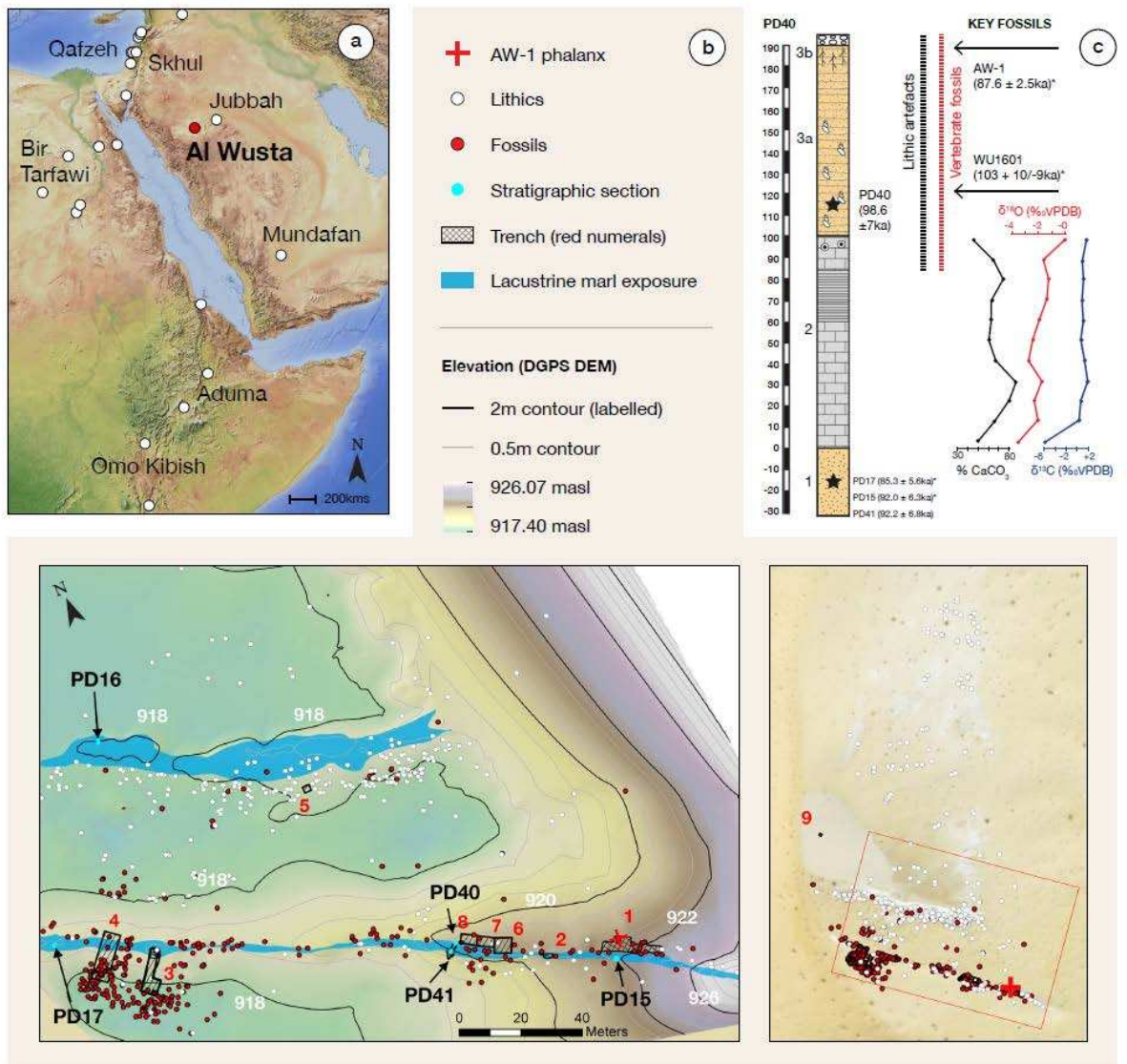
- 870 68. Stoops, G. *Interpretation of micromorphological features of soils and regoliths*
871 (Elsevier, 2010).
- 872 69. Rengberg, I. A procedure for preparing large sets of diatom sets from sediment. *J.*
873 *Palaeolimnol* **4**, 87-90 (1990).
- 874 70. Battarbee, R. W., Knen, M. J. The use of electronically counter microspheres in
875 absolute diatom analysis. *Limnol. Oceanogr.* **27**, 184-188 (1982).
- 876 71. Krammer, K., Lange-Bertalot, H. *Bacillariophyceae 2. Teil Epithemiaceae,*
877 *Suirellaceae* (Gustav-Fisher Verlag, 1988).
- 878 72. Krammer, K., Lange-Bertalot, H. *Bacillariophyceae 3. Teil Centrales,*
879 *Fragicariaceae, Eunotiaceae* (Gustav-Fisher Verlag, 1991a).
- 880 73. Krammer, K., Lange-Bertalot, H. *Bacillariophyceae 4. Teil Achnantheaceae, Kribshe*
881 *Ergänzungen zu Navicula (Lineolate) und Gomphonema* (Gustav-Fisher Verlag,
882 1991b).
- 883 74. Crawford, R. M., Likhoshway, Y. V., Jahn, R. Morphology and identity of
884 *Aulacoseira italic* and typification of *Aulacoseira* (Bacillariophyta). *Diatom*
885 *Research* **18**, 1-19 (2003).
- 886 75. Navok, T., Guillory, W. X., Julius, M. L., Theriort, E. C., Alverson, A. J. Towards a
887 phylogenetic classification of species belonging to the diatom genus *Cyclotella*
888 (Bacillariophyceae): Transfer of species formerly placed in *Puncticulata,*
889 *Handmannia, Pliocaenicus* and *Cyclotella* to the genus *Lindavia*. *Phytotaxa* **217**, 249-
890 264 (2015).
- 891 76. Ter Braak, C. J. F., Šmilauer, P. *CANOCO reference manual and CanoDraw for*
892 *Windows user's guide: software for canonical community ordination (version 4.5).*
893 (Microcomputer Power, 2002).

- 894 77. Hill, M. O., Gauch, H. G. Detrended correspondence analysis: An improved
895 ordination technique. *Plant. Ecol.* **42**, 47-58 (1980).
- 896 78. Ter Braak, C. J. F., Prentice, I. C. A theory of gradient analysis. *Adv. Ecol. Res.* **18**,
897 271-317 (1988).
- 898 79. Ter Braak, C. J. F. Canonical Correspondence Analysis: A new eigenvector technique
899 for multivariate direct gradient analysis. *Ecology* **67**, 1167-1179 (1986).
- 900 80. Smol, J. P. et al. Climate-driven regime shifts in the biological communities of arctic
901 lakes. *Proc. Natl. Acad. Sci. USA* **102**, 4397-4402 (2005).
- 902 81. Birks, H. J. B., Gordon, A. D. *Numerical methods in Quaternary Pollen Analysis*.
903 (Academic Press, 1985).
- 904 82. Juggins, S. *ZONE software, version 1.2*. (University of Newcastle, 1985).
- 905 83. Bennett, K. D. Determination of the number of zones in a biostratigraphical sequence.
906 *New Phytologist* **132**, 155-170 (1996).
- 907 84. Ryves, D. B. Juggins S., Fritz, S. C., Battarbee, R. W. Experimental diatom
908 dissolution and the quantification of microfossil preservation in sediments.
909 *Palaeogeogr. Palaeoclimatol. Palaeoecol.* **172**, 99-113 (2001).
- 910 85. Candy, I. et al. The evolution of Palaeolake Flixton and the environmental context of
911 Starr Carr: an oxygen and carbon isotopic record of environmental change for the
912 early Holocene. *Proc. Geol. Assoc.* **126**, 60-71 (2015).
- 913 86. Domínguez-Rodrigo, M., Barba, R., De la Torre, I., Mora, R. in *Deconstructing*
914 *Olduvai: A Taphonomic Study of the Bed I Sites* (eds. Domínguez-Rodrigo, M.,
915 Barba, R., Egeland, C. P.) 101-125 (New York, Springer, 2007).
- 916 87. Bunn, H. T. *Meat-eating and human evolution: Studies on the diet and subsistence*
917 *patterns of Plio-Pleistocene hominids in East Africa* (University of Wisconsin,
918 Madison, Unpublished PhD thesis, 1982).

- 919 88. Bunn, H. T., Kroll, E. M. Systematic butchery by Pilo/ Pleistocene Hominids at
920 Olduvai Gorge , Tanzania. *Curr. Anthropol.* **27**, 431–452 (1986).
- 921 89. Binford, L. R. *Faunal remains from Klasies River Mouth*. (Academic Press, 1984).
- 922 90. Andrews, P. & Cook, J. Natural modifications to bones in a temperature setting. *Man*
923 **20**, 675–691 (1985).
- 924 91. Blumenschine, R. J., Selvaggio, M. M. Percussion marks on bone surfaces as a new
925 diagnostic of hominid behaviour. *Nature* **333**, 763–765 (1988).
- 926 92. Fisher, J. W. Bone Surface modifications in zooarchaeology. *J. Archaeol. Method*
927 *Theory* **2**, 7–68 (1995).
- 928 93. Noe-Nygaard, N. Man-made trace fossils on bones. *J. Hum. Evol.* **4**, 461–461 (1989).
- 929 94. Binford, L. R. *Bones: Ancient Men and Modern Myths*. (Academic Press, 1981).
- 930 95. Stiner, M., Kuhn, S., Weiner, S., Bar-Yosef, O. Differential burning, recrystallization,
931 and fragmentation of archaeological bone. *J. Archaeol. Sci.* **22**, 223–237 (1995).
- 932 96. Shipman, P., Foster, G., Schoeninger, M. Bunt bones and teeth: an experimental study
933 of color, morphology, crystal structure and shrinkage. *J. Archaeol. Sci.* **11**, 307–325
934 (1984).
- 935 97. Tong, H. W., Zhang, S., Chen, F., Li, Q. Rongements sélectifs des os par les porcs-
936 épics et autres rongeurs : cas de la grotte Tianyuan, un site avec des restes humains
937 fossiles récemment découvert près de Zhoukoudian (Choukoutien). *Anthropologie*
938 **112**, 353–369 (2008).
- 939 98. Dart, R. A. Bone tools and Porcupine gnawing. *Am. Anthropol.* **60**, 715–724 (1958).
- 940 99. Behrensmeier, A. K. Taphonomic and ecological information from bone weathering.
941 *Paleobiology* **4**, 150–162 (1978).
- 942 100. Behrensmeier, A. K., Gordon, K., Yanagi, G. T. Trampling as a cause of bone
943 surface damage and psuedo-cutmarks. *Nature* **319**, 402–403 (1986).

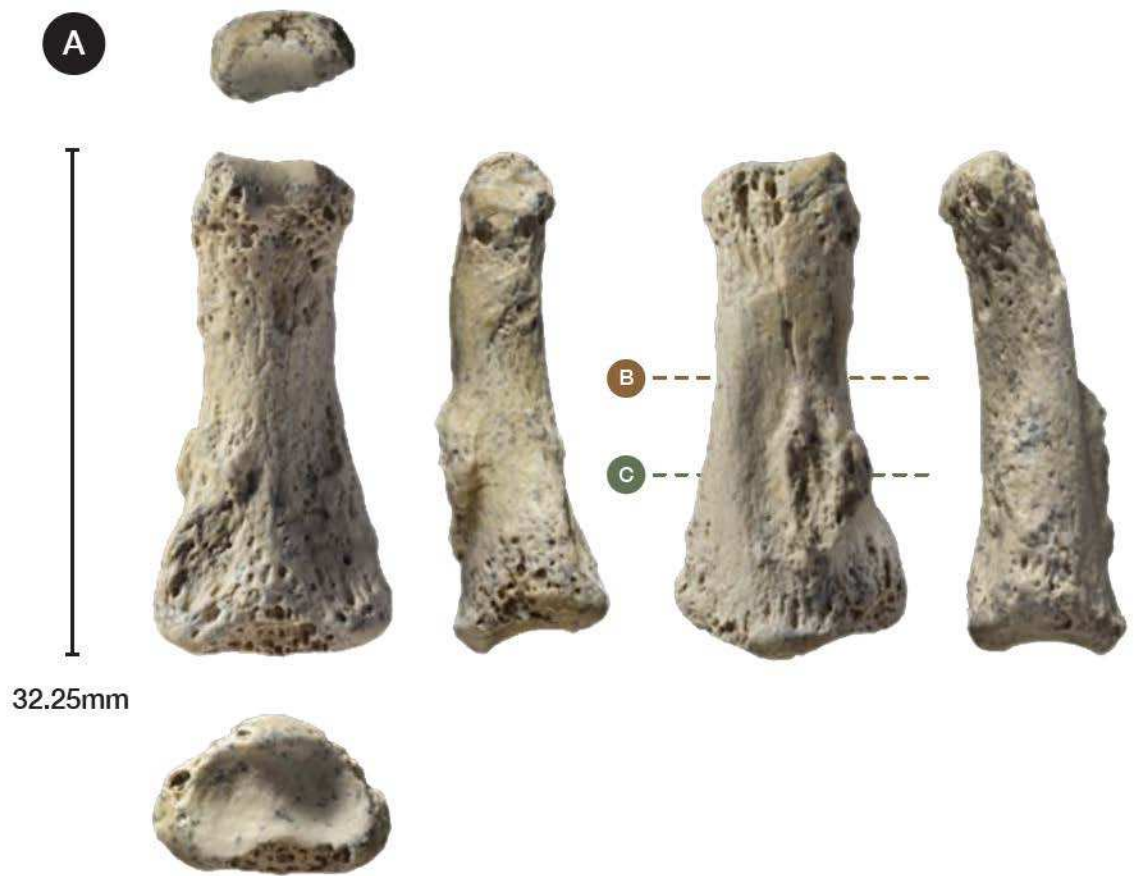
- 944 101. Villa, P., Mahieu, E. Breakage pattern of human long bones. *J. Hum. Evol.* **21**,
945 27–48 (1991).
- 946 102. Bunn, H. T. in *Animals and Archaeology, Volume 1* (eds. Clutton-Brock, J. &
947 Grigson, C.) **1977**, 143–148 (Oxford, BAR International Series 163, 1983).
- 948 103. Scerri, E. M. L., Groucutt, H. S., Jennings, R. P., Petraglia, M. D. Unexpected
949 technological heterogeneity in northern Arabia indicates complex Late Pleistocene
950 demography at the gateway to Asia. *J. Hum. Evol.* **75**, 125-142 (2014).
- 951 104. Scerri, E. M. L., Gravina, B., Blinkhorn, J., Delagnes, A. Can lithic attribute
952 analyses identify discrete reduction trajectories? A quantitative study using refitted
953 lithic sets. *J. Arch. Method Theory* **23**, 669-691 (2016).
- 954 **105.** Groucutt, H.S., et al. Late Pleistocene lakeshore settlement in northern Arabia:
955 Middle Palaeolithic technology from Jebel Katefeh, Jubbah. *Quatern. Int.* **382**, 215-
956 236 (2016).
- 957

Figure 1

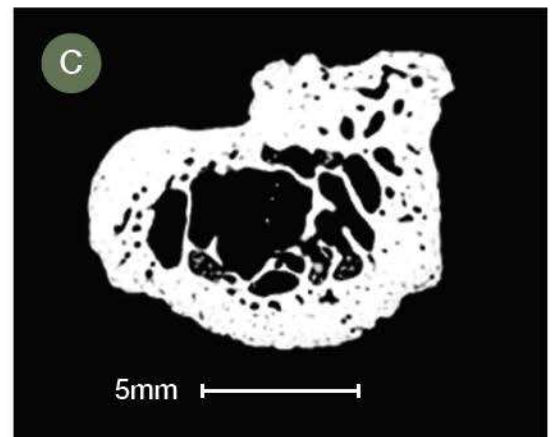
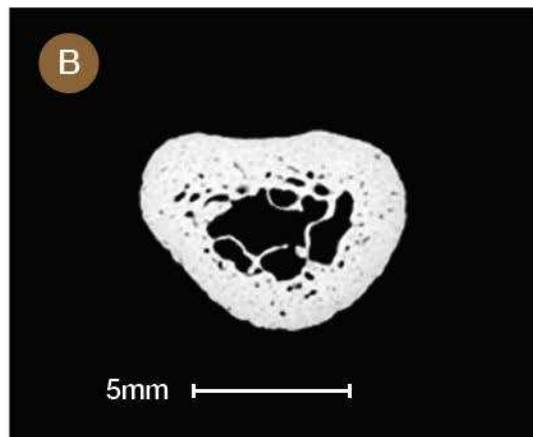


961

Figure 2



32.25mm

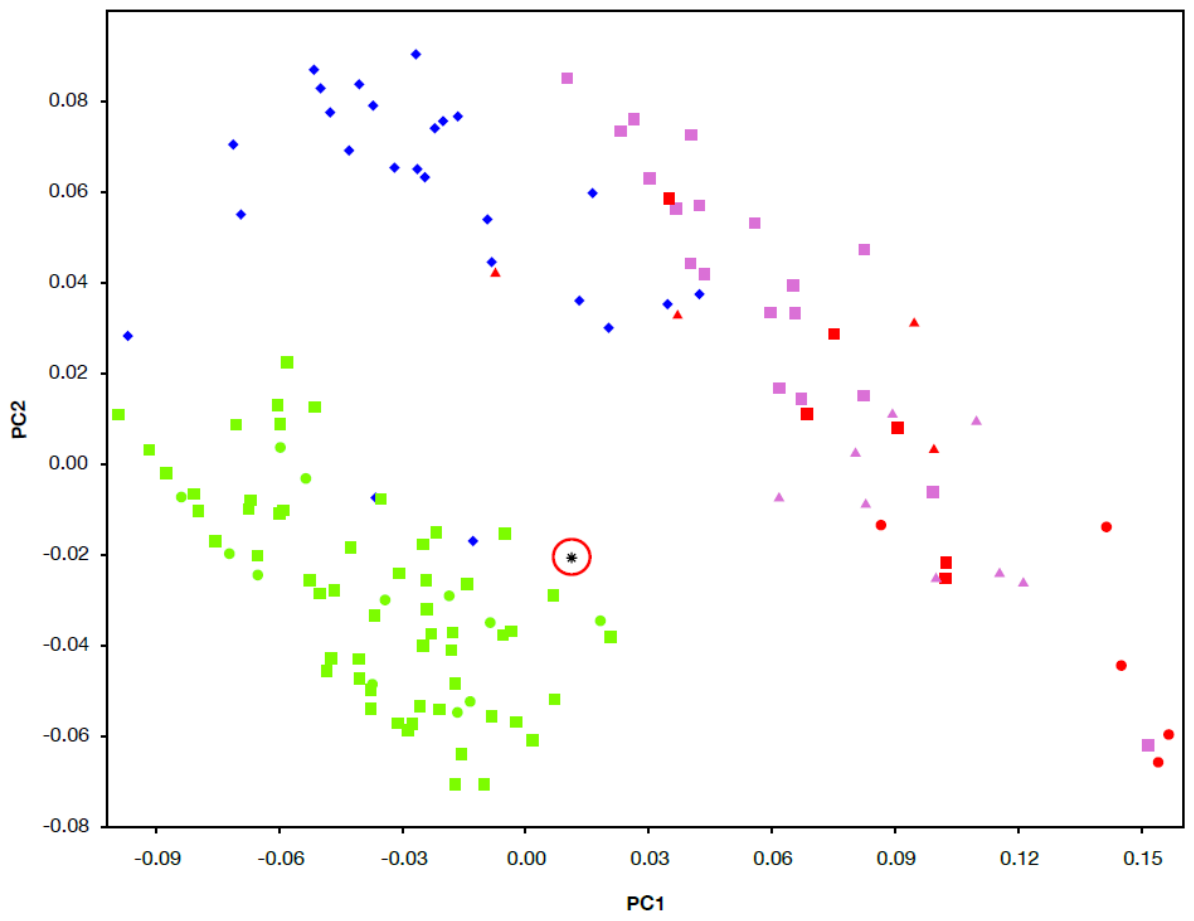


962

963

964

Figure 3

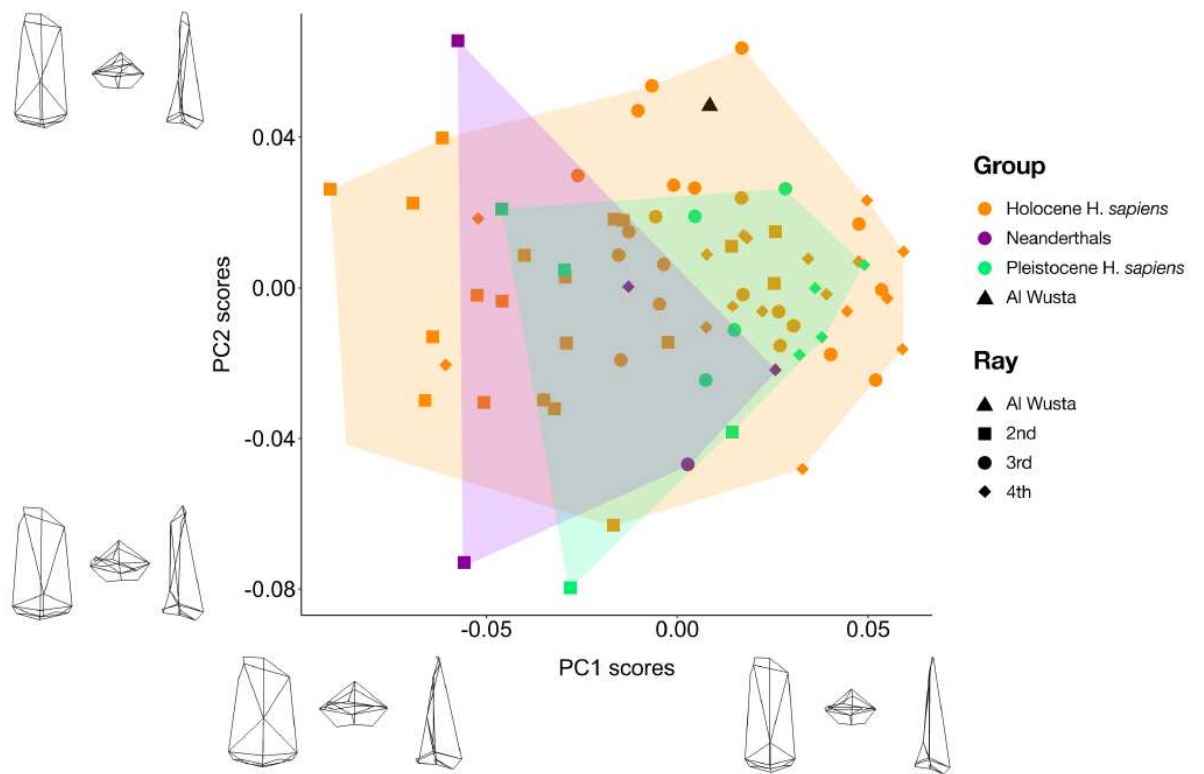


965

966

967

Figure 4



968

969

Figure 5

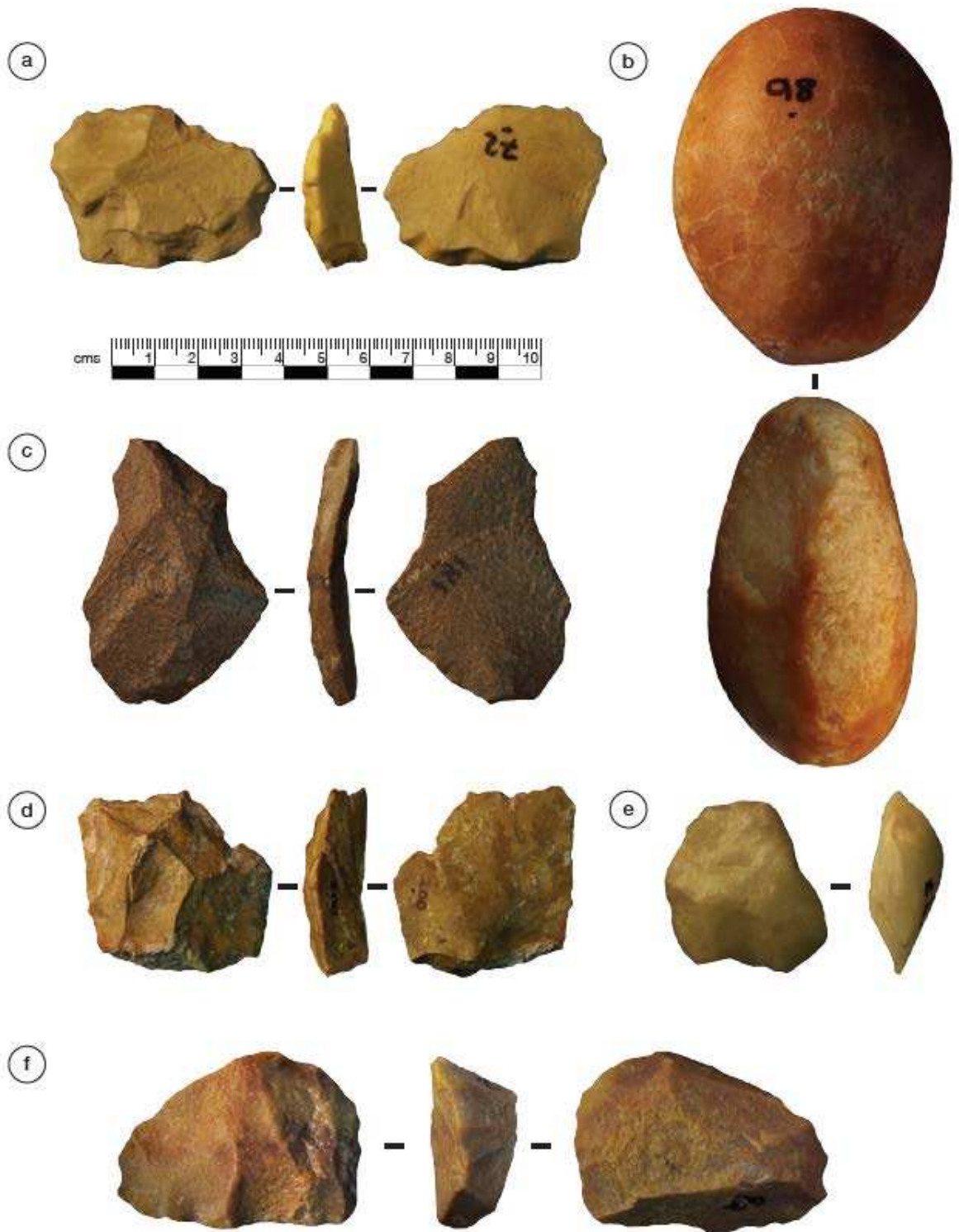


Figure 6

